DR-MMC Hub Based Hybrid AC/DC Collection and HVDC Transmission System for Large-scale Offshore Wind Farms

Wang Xiang, *Member*, *IEEE*, Mingrui Yang, and Jinyu Wen, *Member*, *IEEE*

***Abstract*—Conventional offshore wind farm (OWF) integration systems typically employ AC cables to gather power to a modular multilevel converter (MMC) platform, subsequently delivering it to onshore grids through high-voltage direct current (HVDC) transmission. However, scaling up the capacity of OWFs introduces significant challenges due to the high costs associated with AC collection cables and offshore MMC platforms. This paper proposes a diode rectifier (DR)-MMC hub based hybrid AC/DC collection and HVDC transmission system for large-scale offshore wind farms. The wind farms in proximity to the offshore converter platform utilize AC collection, while distant wind farms connect to the platform using DC collection. The combined AC/DC power is then transmitted to the offshore DR-MMC hub platform. The topology and operation principle of the DR-MMC hub as well as the integration system are presented. Based on the operational characteristics, the capacity design method for DR-MMC hub is proposed. And the control and startup strategies of the integration system are designed. Furthermore, an economic comparison with the conventional MMC-HVDC based offshore wind power integration system is conducted. Finally, the technical feasibility of the proposed integration scheme is verified through PSCAD/EMTDC simulation with the integration scale of 2 GW.**

***Index Terms*—Offshore wind farm, hybrid AC/DC collection, diode rectifier (DR), modular multilevel converter (MMC), high-voltage direct current (HVDC), integration system.**

I. Introduction

ACCORDING to the Global Wind Energy Council, over 380 GW offshore wind power is expected to be installed worldwide in the next decade [1]. For long-distance and deep-sea offshore wind farms (OWFs), the modular multilevel converter based high-voltage direct current (MMC-HVDC) technology is the most commonly used, such as the Borwin3 and DolWin3 projects with a standard high-voltage direct current (HVDC) voltage of ±320 kV and a transmission capacity of 900 MW [2], [3].

To reduce the cost of the integration system, one approach is to optimize the investments of the offshore step-up transformer platform. Borwin5-6 and Dolwin5 projects adopt 66 kV AC collection, which connects offshore AC wind farms directly to offshore converter platforms via 66 kV submarine cables, avoiding the construction of the offshore step-up transformer platform. The other approach is to reduce the cost of the offshore converter platform. Compared with modular multilevel converter (MMC), the diode rectifier (DR) converter offers lower investment cost with smaller size [4]. However, the uncontrolled nature of DR mandates a stable AC voltage for effective operation [5]. Therefore, various hybrid converters combining DR and MMC have been proposed, which utilize MMC to provide the stable AC voltage required for DR operation. Reference [6] proposes a parallel structure of DR and MMC for offshore converter platforms, while [7] proposes a DR-MMC series structure. The investment costs for both types of offshore converter platforms mentioned above are effectively reduced.

As the scale of OWFs increases, the length of AC collection networks increases, resulting in a significant increase in costs and transmission losses [8] of AC collection system. In contrast to the conventional AC collection, DC collection has a high transmission capacity and a lower transmission loss, which has received increased attention [9]. There are two typical DC collection schemes. One is to directly connect multiple DC wind turbines (WTs) in series to increase the collection voltage from medium-voltage direct current (MVDC) to HVDC for transmission [10]. The other is to connect DC WTs in parallel and subsequently centrally boost the voltage to HVDC through an offshore DC/DC converter station [11]. Based on the two schemes, several other DC collection schemes have also been researched. References [12] and [13] introduce a series-parallel DC collection topology, eliminating the need for a centralized offshore DC/DC converter station and enhancing the operational reliability. Reference [14] proposes a distributed DC collection topology, connecting multiple DC WTs to a cascaded distributed DC/DC converter for HVDC transmission. However, all these DC collection approaches necessitate a substantial number of DC/DC converters, leading to increased investment costs and challenges in coordinated control. Currently, there are no operational offshore wind power projects employing DC collection and HVDC transmission.

Manuscript received: March 2, 2024; revised: May 27, 2024; accepted: June 14, 2024. Date of CrossCheck: June 14, 2024. Date of online publication: July 23, 2024.

This work was supported by the National Key Research and Development Program of China (No. 2022YFB2405400).

W. Xiang (corresponding author), M. Yang, and J. Wen are with the School of Electrical and Electronic Engineering, Huazhong University of Science and Technology, Wuhan 430074, China (e-mail: xiangwang1003@hust.edu.cn; myrang_ee@163.com; jinyu.wen@hust.edu.cn).

DOI: 10.35833/MPCE.2024.000229

In order to overcome the above problem, this paper proposes a DR-MMC hub based hybrid AC/DC collection and HVDC transmission system for large-scale OWFs. The OWFs in proximity to the offshore hub platform are integrated by adopting AC collection cables, while the remaining remote OWFs are integrated with DC collection cables. To optimize the cost of the offshore converter platform, the DR is introduced to form a DR-MMC based multiport hub for power transmission. The main contributions of this paper are outlined as follows.

1) A DR-MMC hub based hybrid AC/DC collection and HVDC transmission system is proposed for large-scale offshore wind power integration. Compared with existing offshore wind power integration schemes, this integration scheme has lower investment costs and operation losses.

2) For the proposed integration scheme, a parameter optimization design method for the DR-MMC hub is proposed. The system parameters can be designed based on this method to minimize the operation loss.

3) A dual grid-forming control strategy is proposed for the offshore MMC station. Different from the conventional AC grid-forming control, the dual grid-forming control can provide stable integration voltage for both AC and DC wind farms simultaneously.

4) A startup strategy is proposed for the integration system, which overcomes the issue of the difficulty in black-start due to the unidirectional conductivity of DR.

The remainder of this paper is organized as follows. The topology and operation principle of the DR-MMC hub based hybrid AC/DC collection and HVDC transmission system are introduced in Section II. Then, the control design for the proposed DR-MMC hub based hybrid AC/DC collection and HVDC transmission system is presented in Section III. In Section IV, the parameter design of the integration system is carried out. And the economic evaluation is also elaborated. A startup strategy of the integration system is introduced in Section V. The simulation validation is provided in Section VI. Finally, conclusions are drawn in Section VII.

II. Topology and Operation Principle of DR-MMC Hub Based Hybrid AC/DC Collection and HVDC Transmission System

A. Topology of Proposed Offshore Wind Farm Integration System

Figure 1 illustrates the configuration of the hybrid AC/DC collection and HVDC transmission system designed for large-scale OWFs. The system is comprised of offshore AC and DC wind farms, AC and DC collection networks, an offshore DR-MMC three-port AC/DC/DC hub (abbreviated as DR-MMC hub), and HVDC submarine cables.

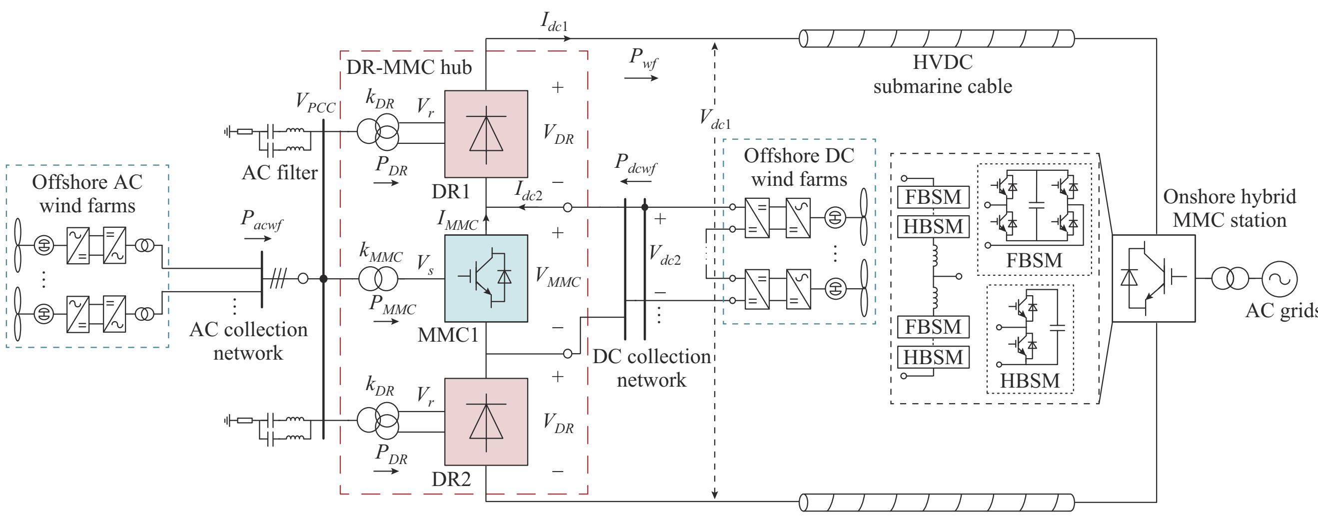

Fig. 1. Topology diagram of proposed hybrid AC/DC collection and HVDC system for large-scale offshore wind power integration.

The key component facilitating AC/DC power conversion is the proposed DR-MMC hub, outlined with the red dashed box in Fig. 1. The hub comprises MMC1, DR1, and DR2. On the AC side, MMC1, DR1, and DR2 are interconnected in parallel, thereby forming the AC input port of the DR-MMC hub. The DC terminal of MMC1 serves as the DC input port of the DR-MMC hub. The offshore AC wind farms are directly connected to the AC input port through a 66 kV AC collection network, while the offshore DC wind farms are collected to the DC input port via MVDC collection cables. The accumulated AC/DC power is conveyed through the DC output port of the DR-MMC hub and transmitted to the onshore hybrid MMC station via HVDC submarine cables.

In the DR-MMC hub, the circuit structure and parameters of DR1 and DR2 are the same. They both employ a 12-pulse rectifier circuit structure and are equipped with double-tuned AC filters to suppress the 11^{th} and 13^{th} harmonics [15]. The AC WT in the offshore AC wind farms comprises a direct-drive permanent magnet synchronous generator (PMSG), a machine side converter (MSC), a capacitor, a grid side converter (GSC), and a transformer. The rated capacity and output voltage of the AC WT are 10 MW and 66 kV, respectively. In contrast, the DC WT, adapted from the AC counterparts, incorporates a DC/DC converter consisting of two voltage source converters (VSCs) and an AC transformer. Multiple DC WTs with a rated capacity of 16 MW and ±20 kV output voltage are interconnected in series and parallel in the offshore DC wind farms.

Furthermore, in order to achieve the black start of the integration system from onshore power grids, the onshore hybrid MMC station adopts the structure consisting of full-bridge sub-modules (FBSMs) and half-bridge sub-modules (HBSMs). The specific startup strategy of the integration system will be discussed later.

B. Operation Principle

The AC side voltages of MMC1 and two DRs are represented as V_s and V_r, respectively. Correspondingly, the DC side voltages of MMC1 and two DRs are represented as V_{MMC} and V_{DR}, respectively. The DC voltage of the HVDC submarine cable is denoted as V_{dc1}, while the voltage of the DC collection network is denoted as V_{dc2}. As shown in Fig. 1, the AC and DC port voltages of the hub satisfy:

$$\begin{cases} V_s = k_{MMC} V_{PCC} \\ V_r = k_{DR} V_{PCC} \end{cases} \tag{1}$$

$$V_{dc1} = V_{MMC} + 2V_{DR} \tag{2}$$

where V_{PCC} is the voltage at the point of common coupling (PCC) of the AC collection network; and k_{MMC} and k_{DR} are the voltage ratios of the high-voltage side windings to the low-voltage side windings of the interfacing transformers of MMC1 and two DRs, respectively.

Denote the transmitted power of the AC wind farms as P_{acwf} and the power of the DC wind farms as P_{dcwf}. Assuming that the voltage drops of the DC collection network and HVDC submarine cable are negligible, it follows that V_{MMC} equals V_{dc2}. Taking the power flow direction shown in Fig. 1 as the positive direction, the DC currents can be expressed as:

$$\begin{cases} I_{dc1} = \dfrac{P_{wf}}{V_{dc1}} \\ I_{dc2} = \dfrac{P_{dcwf}}{V_{dc2}} \\ I_{MMC} = I_{dc1} - I_{dc2} = \dfrac{P_{wf}}{V_{dc1}} - \dfrac{P_{dcwf}}{V_{dc2}} \end{cases} \tag{3}$$

where P_{wf} is the total power of the AC and DC wind farms; I_{dc1} is the current of the HVDC submarine cable; I_{dc2} is the current of the DC collection network; and I_{MMC} is the DC side current of MMC1.

In order to analyze the operation principle of the proposed DR-MMC hub, the DC voltage ratio n and the active power ratio α are defined as:

$$n = \frac{V_{MMC}}{V_{dc1}} \quad 0 < n < 1 \tag{4}$$

$$\alpha = \frac{P_{dcwf}}{P_{wf}} \quad 0 \le \alpha \le 1 \tag{5}$$

Based on (1)-(5), the active power of MMC1, DR1, and DR2 are calculated as:

$$P_{MMC} = V_{MMC} I_{MMC} = \frac{V_{MMC}}{V_{dc1}} P_{wf} - P_{dcwf} = \frac{V_{MMC}}{V_{dc1}} P_{acwf} - \frac{2V_{DR}}{V_{dc1}} P_{dcwf} = nP_{acwf} - (1-n) P_{dcwf} = (n-\alpha) P_{wf} \tag{6}$$

$$P_{DR} = V_{DR} I_{dc1} = \frac{V_{DR}}{V_{dc1}} P_{wf} = \frac{V_{DR}}{V_{dc1}} (P_{acwf} + P_{dcwf}) = \frac{1-n}{2} P_{wf} \tag{7}$$

where P_{MMC} and P_{DR} are the active power of MMC1 and two DRs, respectively.

It can be observed from (6) and (7) that the transmitted power from the AC and DC wind farms counteracts at MMC1. When n equals α, P_{MMC} is equal to 0. While the transmitted power from the AC and DC wind farms is superposed at DR. Denote the operation power of the DR-MMC hub as P_{hub}, which can be calculated based on (6) and (7) as:

$$P_{hub} = P_{MMC} + 2P_{DR} = \begin{cases} (1-\alpha) P_{wf} & P_{MMC} \ge 0 \\ (1+\alpha-2n) P_{wf} & P_{MMC} < 0 \end{cases} \tag{8}$$

Given that $0 \le \alpha \le 1$, it can be observed from (8) that P_{hub} is always less than P_{wf} when P_{MMC} is positive. When P_{MMC} is negative, P_{hub} will be lower than P_{wf} if $1+\alpha-2n$ is less than 1. Consequently, when α and n are within an appropriate range, P_{hub} will be less than the total transmitted power of wind farms, which contributes to a reduction in the operation loss of the integration system.

III. Control Design of DR-MMC Hub Based Hybrid AC/DC Collection and HVDC Transmission System

A. Control Strategy of Offshore AC and DC Wind Farms

Figure 2 illustrates the topology and control strategy of AC and DC WTs, where V_C is the DC voltage of the capacitor in WT; and V_T is the voltage of the high-voltage side windings of the AC transformer in DC WT. As shown in Fig. 2 (a), the AC power is generated through the rotation of PMSG, and then subsequently transmitted via the MSC, GSC, and transformer. MSC adopts the maximum power point tracking (MPPT) control to optimize the harnessing of wind energy, while GSC employs DC voltage control to maintain the DC link voltage.

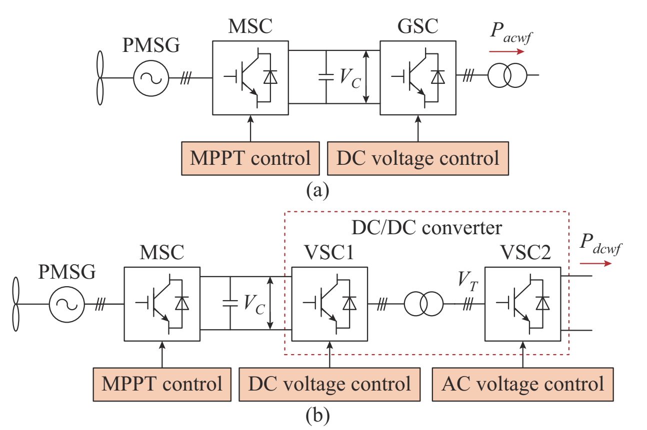

Fig. 2. Topology and control strategy of AC and DC WTs. (a) AC WT. (b) DC WT.

In contrast to the AC WT, the DC WT utilizes a DC/DC converter to generate DC power, which is illustrated in the red dashed box in Fig. 2(b). The VSC1 adopts DC voltage control to maintain the DC link voltage, while VSC2 adopts AC voltage control to maintain the AC voltage of the transformer winding.

B. Dual Grid-forming Control of Offshore MMC1

Both the AC and DC WTs adopt the conventional grid-following control, indicating that the offshore MMC1 must be capable of forming AC and DC network voltages to facilitate the integration of corresponding wind farms.

Considering that the onshore hybrid MMC station regulates V_{dc1} as a constant value by DC voltage control, the DC side voltages of MMC1 and two DRs are coupled with each other according to (2). For DR, the voltages on its AC and DC sides satisfy:

$$V_{DR}=\frac{6\sqrt{2}}{\pi}V_r-\frac{6}{\pi}X_rI_{dc1} \tag{9}$$

where X_r is the leakage reactance of the interfacing transformers of two DRs.

It can be observed from (9) that V_{DR} is determined by V_r and I_{dc1}. Figure 3 illustrates the variation of the DC side voltage of MMC1 and two DRs when the wind farm power fluctuates. Assuming that the total power of the wind farms increases, I_{dc1} will also increase, given that V_{dc1} remains constant. According to (9), if V_r is constant, an increase in I_{dc1} will result in a decrease in V_{DR}. Consequently, the decrease in V_{DR} will cause an increase in V_{MMC} according to (2). It may cause the DC wind farm to disconnect when V_{MMC} changes drastically.

$$P_{wf}\uparrow \xrightarrow{\text{Equation (3)}} I_{dc1}\uparrow \xrightarrow{\text{Equation (9)}} V_{DR}\downarrow \xrightarrow{\text{Equation (2)}} V_{MMC}\uparrow$$

Fig. 3. Variation of V_{MMC} and V_{DR} when wind farm power fluctuates.

Based on the analysis conducted above, MMC1 needs to respond quickly to maintain the stability of its DC side voltage V_{MMC} during wind farm power fluctuations. Based on (2), (3), and (9), V_{MMC} can be calculated as:

$$\begin{aligned}V_{MMC}&=V_{dc1}-\frac{12\sqrt{2}}{\pi}V_r+\frac{12}{\pi}X_rI_{dc1}=\\&V_{dc1}-\frac{12\sqrt{2}}{\pi}k_{DR}V_{PCC}+\frac{12}{\pi}X_r\frac{P_{wf}}{V_{dc1}}\end{aligned} \tag{10}$$

Equation (10) implies that when the transmission power of OWFs P_{wf} increases, the PCC voltage V_{PCC} can be adjusted to increase in order to maintain the stability of the DC side voltage of MMC1 V_{MMC} when the transmission power decreases. Conversely, V_{MMC} can be kept stable by reducing V_{PCC}, when the transmission power decreases. This regulatory process serves as a theoretical foundation for the control design of MMC1.

Based on the above analysis, a dual grid-forming control with AC and DC grid-forming capability is designed for offshore MMC1, as depicted in Fig. 4, where V_d and V_q are the d- and q-axis components of V_{PCC}, respectively; ΔV_{dref} is the additional reference value of the d-axis components of V_{PCC}; I_d and I_q are the d- and q-axis components of the AC current of MMC1, respectively; M_d and M_q are the d- and q-axis components of the AC modulation ratio of MMC1, respectively; L is the sum of the transformer inductance and the arm inductance; f and ω are the frequency and angular frequency of V_{PCC}, respectively; θ is the reference angle of MMC1 modulation, which is generated by the voltage-controlled oscillator (VCO); and the subscript *ref* indicates the reference value of the corresponding parameter.

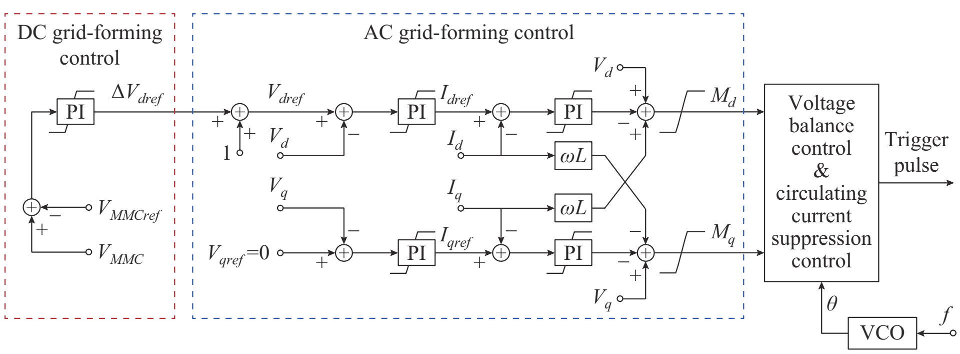

Fig. 4. Dual grid-forming control of offshore MMC1.

As depicted in Fig. 4, the diagram in the orange box represents the DC grid-forming control, while the blue box represents the diagram of the AC grid-forming control. In the DC grid-forming control, the difference between the reference voltage (V_{MMCref}) and the actual voltage (V_{MMC}) is fed into the proportional-integral (PI) regulator, resulting in the output of ΔV_{dref}. The AC grid-forming control utilizes ΔV_{dref} to compute the reference value of the d-axis components of V_{PCC} according to (11).

$$V_{dref}=1+\Delta V_{dref} \tag{11}$$

In summary, the proposed dual grid-forming control has the capability to slightly adjust V_{PCC} when wind farm power fluctuates, thereby maintaining V_{MMC} at a stable value. Consequently, MMC1 can effectively maintain stable AC and DC voltages for AC and DC wind farm integration through the dual grid-forming control.

IV. Parameter Design and Economic Evaluation of Integration System

A. Parameter Design of Integration System

When the values of α and n are appropriate, the operation power of the hub can be reduced to less than the total wind farm power. The decrease of operation power will lead to lower power loss. To determine the values of α and n, according to (6) and (8), the relationship between P_{hub} and P_{wf} can be further expressed as:

$$\frac{P_{hub}}{P_{wf}}=\begin{cases}1-\alpha & \alpha\le n\\ 1+\alpha-2n & \alpha>n\end{cases} \tag{12}$$

The power ratio between P_{hub} and P_{wf} in different operation scenarios is plotted on the orange-red gradient surface of Fig. 5. In order to better show the numerical relationship between P_{hub} and P_{wf}, a gray transparent surface is plotted with $P_{hub}/P_{wf}=1$. The above two surfaces intersect at the red solid line $n=0.5\alpha$. As shown in Fig. 5, when α and n satisfy the condition of (13), P_{hub} is always less than P_{wf}.

$$n>0.5\alpha \tag{13}$$

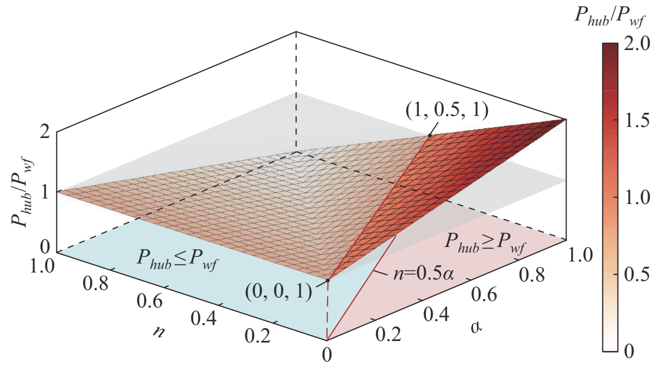

Fig. 5. Power ratio between P_{hub} and P_{wf} versus different power ratio α and DC voltage ratio n.

Based on (13), the values of α and n can be determined to minimize the operation loss of DR-MMC hub. Besides, it is necessary to further optimize the values of α and n with the purpose of reducing the operation loss of MMC1 and DR. Equations (6) and (7) depict the power transmission characteristics of MMC1 and DR. According to (6), the operation power of MMC1 is 0 when $n=\alpha$. Consequently, the operation loss of MMC1 is also 0 in this scenario. And it can be observed from (7) that the operation power of DR is always greater than 0. When n decreases, the operation power of DR increases, with its maximum value being half of P_{wf}.

Based on the above analysis, the DC voltage ratio n and the active power ratio α should be designed as follows:

$$n=\alpha \tag{14}$$

Taking the integration of 2 GW offshore wind power as an example, the rated voltage of HVDC submarine cable is ±500 kV. Considering the constraints of (13) and (14) as well as the typical voltage levels of MVDC systems [16], both α and n can be designed as 0.2. Therefore, the rated DC voltage of MMC1 is ±100 kV. The rated power of AC and DC wind farms is 1600 MW and 400 MW, respectively. The proportion between FBSMs and HBSMs in the onshore hybrid MMC station should be designed as 4:6 according to the rated DC voltage of MMC1. The specific reason will be elucidated in Section V.

Finally, it is necessary to determine the maximum operation power of MMC1 and DR based on the determined α and n. The rated capacity of MMC1 and DR can be determined based on their maximum operation power. Therefore, substituting $\alpha=n=0.2$ into (6) and (7) yields:

$$P_{MMC}=nP_{acwf}-(1-n)P_{dcwf}=0.2P_{acwf}-0.8P_{dcwf}\le 320\text{ MW} \tag{15}$$

$$P_{DR}=\frac{1-n}{2}P_{wf}=0.4P_{wf}\le 800\text{ MW} \tag{16}$$

It can be observed from (15) that offshore MMC1 reaches the maximum operation power of 320 MW when only a single type of OWF is integrated. According to (16), DR reaches the maximum operation power of 800 MW when both the offshore AC and DC wind farms transmit their rated power. Consequently, the rated capacity of offshore MMC1 and DR can be designed as 320 MW and 800 MW, respectively.

B. Economic Evaluation

In order to evaluate the economy of the proposed integration system in the scenario of 2000 MW offshore wind power integration, this subsection compares the cost of the existing AC collection and MMC-HVDC transmission integration system (Scheme I, as shown in Fig. 6) with that of the proposed integration system (Scheme II).

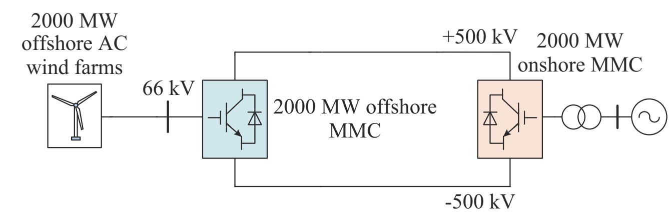

Fig. 6. Topology of AC collection and MMC-HVDC transmission integration system.

As shown in Fig. 6, the difference in component investment costs between the two schemes includes the offshore converter station, onshore converter station, WTs, and collection cables. The initial investment costs of the four parts are calculated as follows.

1) Offshore Converter Station

The cost of the offshore converter station can be calculated by:

$$C_{off,cs}=K_{off,MMC}S_{off,MMC}+K_{off,DR}S_{off,DR} \tag{17}$$

where $C_{off,cs}$ is the total cost of the offshore converter station; $K_{off,MMC}$ and $K_{off,DR}$ are the per-megawatt costs of the offshore MMC and DR stations, respectively; and $S_{off,MMC}$ and $S_{off,DR}$ are the total capacities of MMC and DR stations, respectively.

The cost of the offshore MMC station is about 1.2×10^6 CNY/MW [17]. At the same time, the cost of the offshore DR station is about 35% of the offshore MMC station, i.e., 4.2×10^5 CNY/MW [18].

2) Onshore Converter Station

From Fig. 6, it can be observed that the onshore MMC station in Scheme I adopts the conventional half-bridge (HB) MMC configuration, which is different from the onshore hybrid MMC station in Scheme II. The cost of the onshore converter stations in the two schemes can be respectively calculated by:

$$C_{on,cs}=K_{on,MMC}S_{on,MMC} \tag{18}$$

$$C_{on,cs}=K_{on,hMMC}S_{on,hMMC} \tag{19}$$

where $C_{on,cs}$ is the total cost of the onshore converter station; $K_{on,MMC}$ and $S_{on,MMC}$ are the per-megawatt cost and total capacity of the onshore MMC station in Scheme I, respectively; and $K_{on,hMMC}$ and $S_{on,hMMC}$ are the per-megawatt cost and total capacity of the onshore hybrid MMC station in Scheme II, respectively.

Considering different construction difficulties, the cost of onshore MMC station is lower than that of offshore MMC station. According to [17], the cost of the conventional onshore MMC station is about 9.5×10^5 CNY/MW. It can be calculated from [19] that the cost of the onshore hybrid MMC station in Scheme II is about 1.03×10^6 CNY/MW.

3) WTs

Assuming that the AC WTs in the two schemes are the same, the cost of the offshore WTs can be calculated as:

$$C_{OWF}=K_{acwf}S_{acwf}+K_{dcwf}S_{dcwf} \tag{20}$$

where C_{OWF} is the total cost of the offshore WTs; K_{acwf} and S_{acwf} are the per-megawatt cost and the total capacity of the offshore AC WTs, respectively; and K_{dcwf} and S_{dcwf} are the per-megawatt cost and the total capacity of the offshore DC WTs, respectively.

According to [20], the cost of the 66 kV AC WT and ±20 kV DC WT are about 3.95×10^6 and 4.2×10^6 CNY/MW, respectively.

4) Collection Cables

The cost of the collection cables can be calculated as:

$$C_{cab}=n_1 l_1 C_{cab,AC}+n_2 l_2 C_{cab,DC} \tag{21}$$

where C_{cab} is the total cost of collection cables; $C_{cab,AC}$ is the per-kilometer cost of AC collection cables; $C_{cab,DC}$ is the per-kilometer cost of DC collection cables; n_1 and n_2 are the circuit numbers of AC collection cables and DC collection cables, respectively; and l_1 and l_2 are the average lengths of AC collection cables and DC collection cables, respectively.

Given that a 66 kV AC collection cable allows up to 50 MW power transmission, in Scheme I, $n_1=40$ and $n_2=0$. While in Scheme II, $n_1=32$ and $n_2=2$. $l_1=20$ km in Scheme I, while $l_1=10$ km and $l_2=40$ km in Scheme II. The cost of the 66 kV AC collection cable is about 2.8×10^6 CNY/km, and the cost of ±20 kV DC collection cable is about 5×10^6 CNY/km [21].

Based on (17)-(21) and the given parameters in the two schemes, the result of the economic comparison between the two schemes is shown in Table I.

TABLE I
ECONOMIC COMPARISON OF TWO SCHEMES IN SCENARIO OF 2 GW OFFSHORE WIND POWER INTEGRATION

Scheme	Comparison object	Cost (10^9 CNY)
Scheme I	Offshore converter station	2.400
	Onshore converter station	1.900
	WTs	7.900
	Collection cables	2.240
	Total	14.440
Scheme II	Offshore converter station	1.056
	Onshore converter station	2.060
	WTs	8.000
	Collection cables	1.296
	Total	12.412

Two conclusions can be drawn from Table I.

1) Compared with Scheme I, Scheme II can significantly save 1.344×10^9 CNY for the offshore converter station, attributable to the low cost of DR. While a saving of 1.104×10^9 CNY in the cost of collection cables can be achieved due to the large transmission capacity of DC collection cables.

2) Although the cost of the onshore converter station and WTs in Scheme II slightly increases compared with that in Scheme I, the substantial reduction in the cost of offshore converter station and collection cables leads to a total cost reduction of 2.028×10^9 CNY in Scheme II. It can be observed that Scheme II has significant economic advantages over Scheme I.

V. STARTUP STRATEGY OF INTEGRATION SYSTEM

Due to the unidirectional conductivity of DR, it cannot be directly started from onshore power grids. Therefore, at the initial stage of the startup procedure, DR1 and DR2 need to be bypassed, and the integration system operates as MMC-HVDC at this time. The onshore hybrid MMC needs to reduce its DC voltage to the rated DC voltage of MMC1 (±100 kV) and charge MMC1. For this reason, the ratio of the FBSMs and HBSMs of the onshore hybrid MMC needs to be 4:6 [22].

After MMC1 is started, DR1 and DR2 can be put into operation at AC and DC sides. Then, MMC1 controls the voltage of PCC V_{PCC} from 0 to 1.0 p.u. through AC voltage control. As V_{PCC} rises, the DC voltage of two DRs V_{DR} will also increase. Meanwhile, the onshore hybrid MMC also needs to raise its DC voltage V_{dc1} synchronously to the rated value. The voltage rising process needs to be synchronized to avoid overcurrent. At this moment, the voltage of each port of the hub reaches the rated value. The offshore AC and DC wind farms can be separately connected to the hub for power transmission.

From the above, the startup process of the integration system can be divided into three stages, as shown in Fig. 7(a)-(c). The bypass switches of the integration system are represented by QF1-QF5 in Fig. 7.

1) Stage 1: charge MMC1. As shown in Fig. 7(a), QF1 is closed while other QFs are open, and the system operates as MMC-HVDC.

2) Stage 2: put DR into operation. As shown in Fig. 7(b), once MMC1 is fully charged, open QF1. Concurrently, QF2 and QF3 are closed to put DR into operation. Subsequently, V_{DR} and V_{dc1} will rise synchronously to their respective rated values.

3) Stage 3: integrate OWFs. As shown in Fig. 7(c), after the DR-MMC hub is started, the AC and DC wind farms can be connected to the hub respectively and start transmitting power.

Before the AC and DC wind farms begin to transmit power, the AC and DC WTs need to absorb power from the hub for startup. Taking the DC WTs as an example, VSC2 first deblocks and raises the internal AC voltage V_T of the DC/DC converter to its rated value.

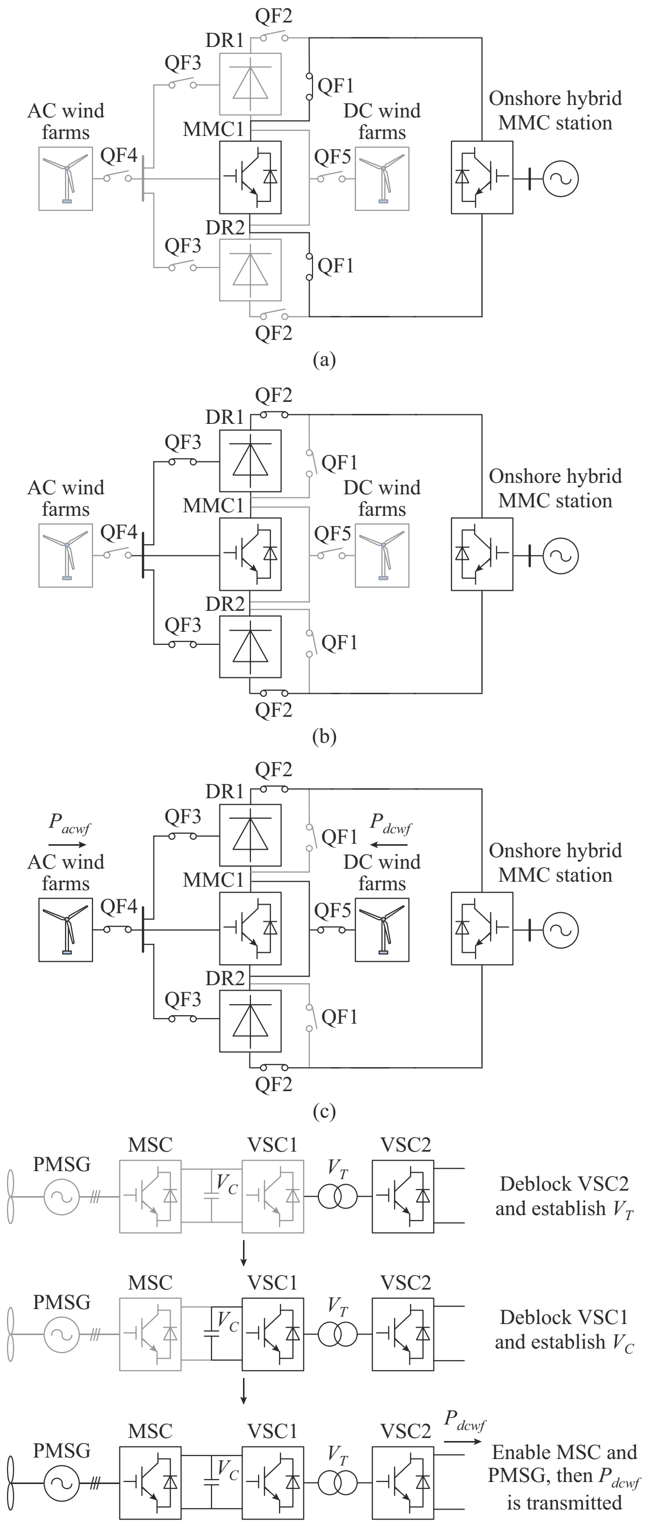

(a) (b) (c) (d)

Fig. 7. Startup process of integration system. (a) Stage 1. (b) Stage 2. (c) Stage 3. (d) Startup process of DC WT.

At this time, since VSC1 is still in the blocked state, the capacitor of the DC WT can only be charged through the uncontrolled DR rectification bridge in VSC1.

After the uncontrolled charging process of the capacitor is completed, VSC1 is enabled and controls the capacitor voltage V_C to rise to the rated value. Finally, the MSC and PMSG can be enabled, and the DC power is transmitted to the hub.

In summary, the startup process of the DC WT can be divided into three steps, as shown in Fig. 7(d).

Step 1: VSC2 is deblocked, and the capacitor is charged uncontrollably.

Step 2: VSC1 is deblocked, and the capacitor voltage rises to the rated value.

Step 3: enable MSC and PMSG, and the power starts to be transmitted to the hub.

It is worth noting that DR necessitates absorbing a specific amount of reactive power during its operation. Consequently, the reactive power capacity of the AC filter should be designed based on the operational needs of two DRs in the hub. Once the wind farms start transmitting power, the AC filter needs to be put into operation. Furthermore, to prevent instantaneous overcurrent during startup, current limiting resistors are installed at MMC1, offshore AC wind farms, and offshore DC wind farms.

VI. Simulation Validation

To test the technical feasibility of the proposed integration scheme, a simulation model of the hybrid AC/DC collection and HVDC transmission system illustrated in Fig. 1 is built in PSCAD/EMTDC. The parameters of the simulation model are given in Table II.

TABLE II
Parameters of Simulation Model

Component	Parameter	Value
AC wind farms	Power rating	1600 MW
	Rated AC voltage	66 kV
	Frequency	50 Hz
	Total length of AC collection cable	320 km
DC wind farms	Power rating	400 MW
	Rated DC voltage	±100 kV
	Total length of DC collection cable	80 km
HVDC transmission	Power rating	2000 MW
	Rated DC voltage	±500 kV
	HVDC transmission cable length	120 km
MMC1	Rated capacity	320 MW
	Rated DC voltage	±100 kV
	Number of sub-module (SM) per arm	100
	Rated SM capacitor voltage	2 kV
	SM capacitance	3.6 mF
	Arm inductance	4.3 mH
	Interfacing transformer voltage ratio	66 kV/105 kV
DR1 and DR2	Rated capacity	800 MW
	Rated DC voltage	400 kV
	Interfacing transformer voltage ratio	66 kV/150 kV/150 kV
	Capacity of AC filter	72 Mvar

Note that the AC collection submarine cables are modeled using a π-equivalent circuit. The DC collection submarine cables are equated by the coaxial cable model. The SM capacitor overvoltage protection threshold and the arm overcurrent protection threshold are set to be 1.5 p.u. and 2 p.u. [23], [24], respectively.

A. Validation of Startup Strategy

To simplify the startup process, it is assumed that the onshore hybrid MMC has been started at the beginning of the simulation and the onshore hybrid MMC has already lowered its DC voltage V_{dc1} to the rated DC voltage of MMC1. In accordance with the startup strategy outlined in Section V, the startup timing sequence of the simulation model is presented in Table III.

TABLE III
STARTUP TIMING SEQUENCE OF SIMULATION MODEL

Time (s)	Event
0	Onshore hybrid MMC reduces DC voltage
0.05	Offshore MMC1 is deblocked and the PCC voltage is controlled at 0
1	DR1 and DR2 are connected at AC and DC sides
1-2	Offshore MMC1 controls PCC voltage to the rated value. DR1 and DR2 are conducted, while the DC voltages of two DRs and onshore hybrid MMC increase synchronously
3-4	AC WTs are deblocked and started. The power of AC wind farms rises to the rated value at 4 s
5-8	DC WTs are deblocked and started. The power of DC wind farms rises to the rated value at 8 s

Figure 8 depicts the simulation results of the proposed integration scheme during the startup process.

Figure 8(a) and (b) shows the charging process of MMC1. It can be observed that the average SM capacitor voltage of MMC1 increases rapidly at the initial stage of the startup process. While the DC voltage of MMC1 quickly rises to the rated value. And it can be observed from Fig. 8(c) that the *d*-axis component of PCC voltage is increased linearly from 0 to 1 p.u. within 1-2 s. Meanwhile, the DC voltages of DRs and onshore hybrid MMC increase synchronously to 400 kV and 1000 kV, respectively, as shown in Fig. 8(d). In Fig. 8(e), the startup procedure of AC wind farms is illustrated. As can be observed, the power of AC wind farms increases from 0 to 1 p.u. within 3-4 s. Figure 8(f) and (h) depicts the startup procedure of DC wind farms. Firstly, the *d*-axis component of the transformer voltage V_T in DC WT increases from 0 to 1 p.u. within 5-5.5 s. Meanwhile, the capacitor voltage V_C in DC WT is charged to 0.77 p.u. through the uncontrolled DR circuit in VSC1, as shown in Fig. 8(g). Then, after VSC2 is deblocked, the capacitor voltage reaches the rated value at 6.2 s. Finally, the power of DC wind farms is increased to 1 p.u. within 7-8 s, as shown in Fig. 8 (h). It can be observed from the simulation results that the startup of the DR-MMC hub, AC wind farms, and DC wind farms can be completed in sequential.

In conclusion, the simulation results in Fig. 8 validate the effectiveness of the proposed startup strategy. In addition, similar to the startup of DC wind farms, the startup of AC wind farms also has the capacitor charging process. However, due to space considerations, the simulation results are omitted.

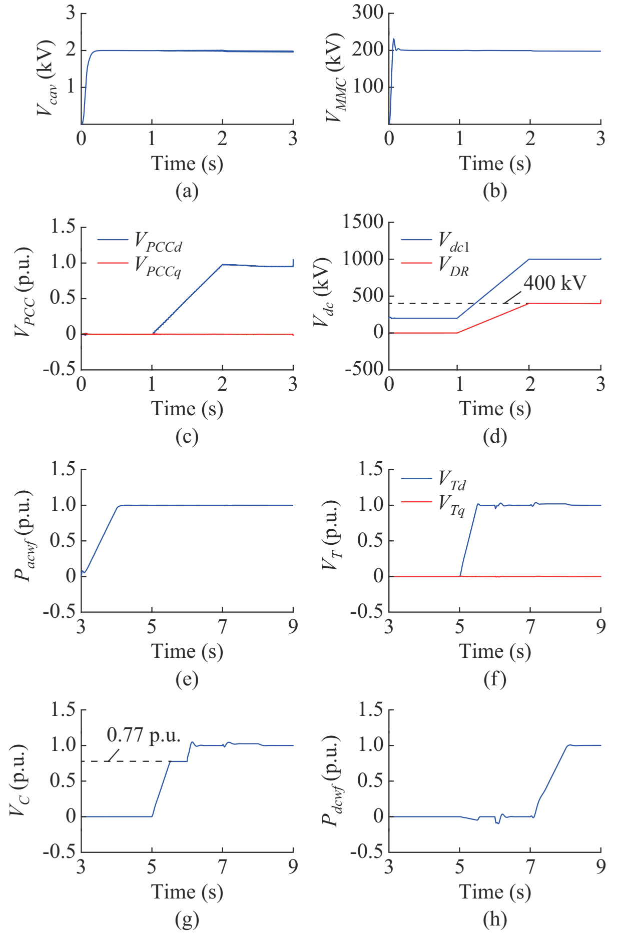

Fig. 8. Simulation results of proposed integration scheme during startup process. (a) Average SM capacitor voltage of MMC1. (b) DC voltage of MMC1. (c) *dq*-axis components of PCC voltage. (d) DC voltage of onshore hybrid MMC and DRs. (e) Power of AC wind farms. (f) *dq*-axis components of VT. (g) Capacitor voltage in DC WTs. (h) Power of DC wind farms.

B. Performance Under Normal Operation

Figure 9 shows the simulation results of the proposed integration scheme under normal operation.

As shown in Fig. 9(a), the power P_{acwf} increases from 0 to 1600 MW within 3-4 s, while the power P_{dcwf} increases from 0 to 400 MW within 7-8 s. During 8-9 s, the integration system is under normal operation with a total power P_{wf} of 2000 MW. Figure 9(b) depicts the active power of MMC1 and two DRs. When only AC wind farms are under rated operation (4-7 s), the active power of MMC1 and DRs is 316 MW and 633 MW, respectively. And when the system is under normal operation (8-9 s), P_{MMC} decreases to almost 0 (–4 MW), while P_{DR} increases to 792 MW. The active power of MMC1 and DRs depicted in Fig. 9(b) verifies the correctness of (6) and (7) in Section II. Furthermore, it can be observed that the total power of the DR-MMC hub P_{hub} with only 1600 MW can provide 2000 MW power (P_{wf}) for the onshore AC grid, which validates the advantages of power characteristics of the DR-MMC hub. As shown in Fig. 9(c) and (d), the *dq*-axis components of the PCC voltage (V_{PCCd} and V_{PCCq}) are maintained at 1 p.u. (66 kV) and 0, respectively, when the system is under normal operation.

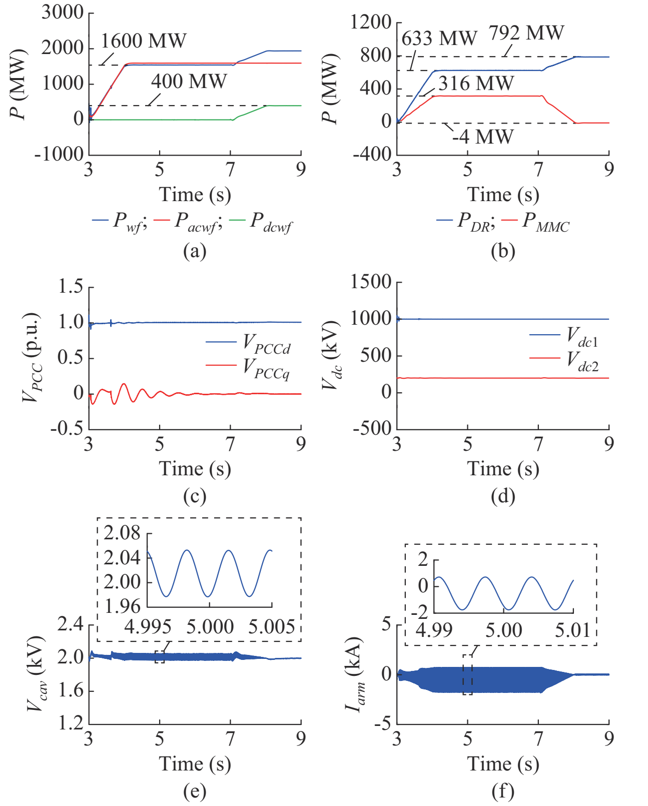

Fig. 9. Simulation results of proposed integration scheme under normal operation. (a) OWF power. (b) Active power of MMC1 and two DRs. (c) *dq*-axis components of PCC voltage. (d) DC voltage. (e) Average SM capacitor voltage of phase A of MMC1. (f) Upper arm current of phase A of MMC1.

Meanwhile, the DC voltages V_{dc1} and V_{dc2} are maintained at their rated values of 1000 kV and 200 kV, respectively. It can be concluded that under normal operation, MMC1 can respectively provide stable AC and DC voltages for the integration of wind farms through the proposed dual grid-forming control. Figure 9(e) and (f) shows the average SM capacitor voltage and the upper arm current of phase A of MMC1, respectively.

Therefore, the simulation results in Fig. 9 confirm that the proposed integration scheme can adapt to the rated 2000 MW AC and DC offshore wind power transmission.

C. Performance Under Wind Power Fluctuation

The dual grid-forming control should effectively maintain the AC and DC voltages (V_{PCC} and V_{dc2}) for the integration of OWFs even when the wind power fluctuates. The simulation results of the proposed integration scheme under wind power fluctuations are shown in Fig. 10, where the left column illustrates the simulation results under the fluctuation of AC wind farms, while the right column shows the simulation results under the fluctuation of DC wind farms. In both cases, the fluctuation of wind power can be described as follows: 1.0 p.u. → 0.5 p.u. ($t=10$ s) → 0.8 p.u. ($t=11$ s) → 0.3 p.u. ($t=12$ s) → 0.6 p.u. ($t=13$ s) → 1.0 p.u. ($t=14$ s).

Figure 10(a) depicts the power fluctuation of both offshore AC and DC wind farms during 10-14 s. As shown in Fig. 10(b) and (c), during wind power fluctuations, the PCC voltage is slightly changed in accordance with the proposed dual grid-forming control. Consequently, the DC voltage V_{dc2} of DR-MMC hub is effectively maintained at its rated value (200 kV). Meanwhile, the DC voltage V_{dc1} is stably controlled at 1000 kV by the onshore hybrid MMC station. As shown in Fig. 10(d) and (e), the average SM capacitor voltage and upper arm current in phase A of MMC1 are within safe operation range under wind power fluctuation.

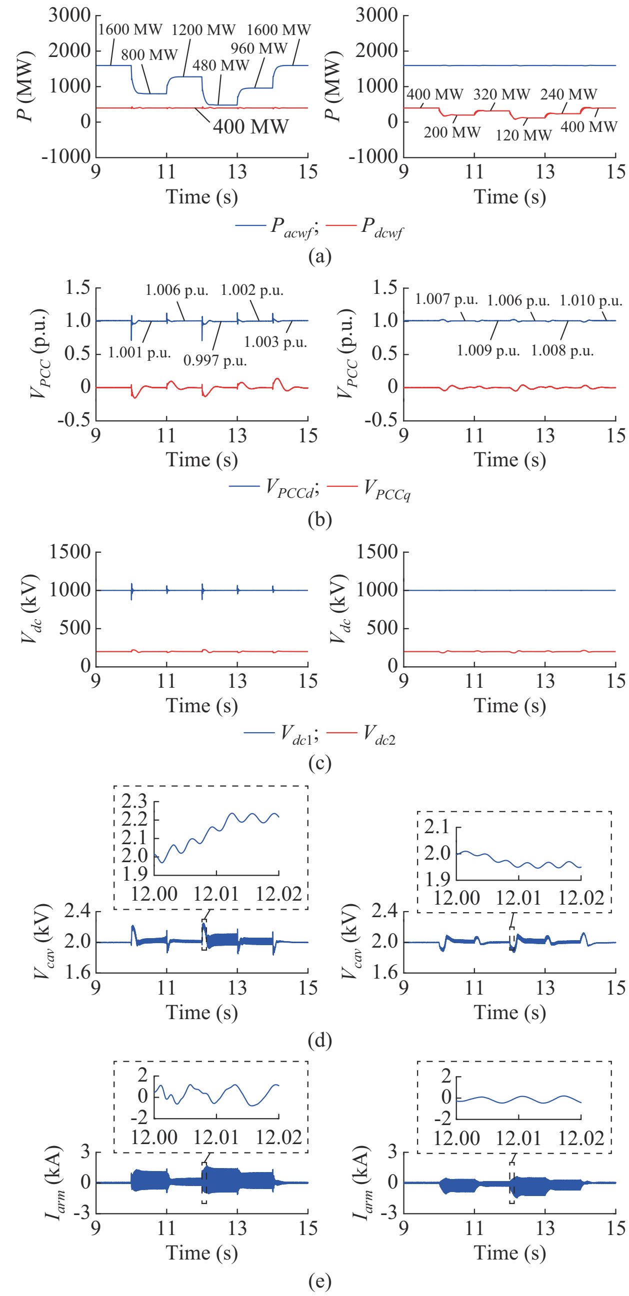

Fig. 10. Simulation results of proposed integration scheme under wind power fluctuations. (a) OWF power. (b) *dq*-axis components of PCC voltage. (c) DC voltage. (d) Average SM capacitor voltage of phase A of MMC1. (e) Upper arm current of phase A of MMC1.

The simulation results depicted in Fig. 10 validate the effectiveness of the proposed dual grid-forming control. Under wind power fluctuations, the integration system can operate well with the dual grid-forming control. Based on the simulation results in Figs. 9 and 10, it can be concluded that the integration system can effectively adapt to both normal and power fluctuation scenarios under the proposed dual grid-forming control.

VII. Conclusion

A DR-MMC hub based hybrid AC/DC collection and HVDC transmission system for large-scale wind power integration is proposed in this paper.

A parameter design method of the integration system is proposed with the objective of reducing power loss. Taking the 2 GW offshore wind power integration as an example, the hub requires only 1600 MW operation power when the DC voltage ratio n equals the power ratio α. Moreover, the economic evaluation demonstrates the proposed integration scheme can reduce the total cost by 2.028×10^9 CNY compared with the existing AC collection and MMC-HVDC transmission scheme.

A dual grid-forming control for the hub is proposed. The simulation results demonstrate that the integration system with this control strategy is capable of maintaining stable operation in both normal and power fluctuation scenarios. Moreover, a startup strategy of the integration system is proposed, which ensures a smooth and steady startup from onshore power grids.

References

[1] GWEC. (2024, Jan.). Global Offshore Wind Report 2023. [Online]. Available: https://gwec.net/gwecs-global-offshore-wind-report-2023/

[2] TenneT. (2023, Dec.). Borwin3. [Online]. Available: https://www.tennet.eu/projects/borwin3

[3] TenneT. (2023, Dec.). Dolwin3. [Online]. Available: https://www.tennet.eu/projects/dolwin3

[4] L. Yu, L. Xu, J. Zhu *et al.*, "Impedance modelling and stability analysis of diode-rectifier based HVDC connected offshore wind farms," *IEEE Transactions on Power Delivery*, vol. 37, no. 1, pp. 591-602, Feb. 2022.

[5] A. Nami, J. L. Rodriguez-Amenedo, S. Arnaltes *et al.*, "Control of the parallel operation of DR-HVDC and VSC-HVDC for offshore wind power transmission," *IEEE Transactions on Power Delivery*, vol. 37, no. 3, pp. 1682-1691, Jun. 2022.

[6] Y. Chang and X. Cai, "Hybrid topology of a diode-rectifier-based HVDC system for offshore wind farms," *IEEE Journal of Emerging and Selected Topics in Power Electronics*, vol. 7, no. 3, pp. 2116-2128, Sept. 2019.

[7] Y. Wu, L. Zhang, Y. Zhou *et al.*, "A hybrid HVDC converter based on MMC and diode rectifier for offshore wind farm integration," in *Proceedings of 2021 International Conference on Power System Technology*, Haikou, China, Dec. 2021, pp. 1476-1480.

[8] M. Gholamian and O. Beik, "Coordinate control of wind turbines in a medium voltage DC grid," *IEEE Transactions on Industry Applications*, vol. 59, no. 5, pp. 6480-6488, Sept. 2023.

[9] W. Liao, Q. Wu, H. Cui *et al.*, "Model predictive control based coordinated voltage control for offshore radial DC-connected wind farms," *Journal of Modern Power Systems and Clean Energy*, vol. 11, no. 1, pp. 280-289, Jan. 2023.

[10] M. Pape and M. Kazerani, "A generic power converter sizing framework for series-connected DC offshore wind farms," *IEEE Transactions on Power Electronics*, vol. 37, no. 2, pp. 2307-2320, Feb. 2022.

[11] K. A. N. Al-Deen and H. A. Hussain, "Review of DC offshore wind farm topologies," in *Proceedings of 2021 IEEE Energy Conversion Congress and Exposition*, Vancouver, Canada, Oct. 2021, pp. 53-60.

[12] H. Zhang, F. Gruson, D. M. F. Rodriguez *et al.*, "Overvoltage limitation method of an offshore wind farm with DC series-parallel collection grid," *IEEE Transactions on Sustainable Energy*, vol. 10, no. 1, pp. 204-213, Jan. 2019.

[13] F. Rong, G. Wu, X. Li *et al.*, "ALL-DC offshore wind farm with series-connected wind turbines to overcome unequal wind speeds," *IEEE Transactions on Power Electronics*, vol. 34, no. 2, pp. 1370-1381, Feb. 2019.

[14] S. Yan, X. Gao, Y. Cui *et al.*, "Study on distributed power-collection and cascaded boosting-voltage topology and strategy for offshore DC station," *IEEE Access*, vol. 11, pp. 23586-23595, Mar. 2023.

[15] R. Li and L. Xu, "A unidirectional hybrid HVDC transmission system based on diode rectifier and full-bridge MMC," *IEEE Journal of Emerging and Selected Topics in Power Electronics*, vol. 9, no. 6, pp. 6974-6984, Dec. 2021.

[16] CIGRE Working Group 31 of Study Committee C6. (2020, Feb.). Medium voltage direct current (MVDC) grid feasibility study. [Online]. Available: https://www.e-cigre.org/publications/detail/793-medium-voltage-direct-current-mvdc-grid-feasibility-study.html

[17] J. Luo, K. Lin, J. Li *et al.*, "Cost analysis and comparison between modular multilevel converter (MMC) and modular multilevel matrix converter (M3C) for offshore wind power transmission," in *Proceedings of 15th IET International Conference on AC and DC Power Transmission*, Coventry, UK, Feb. 2019, pp. 1-6..

[18] Z. Zhang, Y. Jin, and Z. Xu, "Grid-forming control of wind turbines for diode rectifier unit based offshore wind farm integration," *IEEE Transactions on Power Delivery*, vol. 38, no. 2, pp. 1341-1352, Apr. 2023.

[19] P. Meng, W. Xiang, Y. Chi *et al.*, "Resilient DC voltage control for islanded wind farms integration using cascaded hybrid HVDC system," *IEEE Transactions on Power Systems*, vol. 37, no. 2, pp. 1054-1066, Mar. 2022.

[20] J. Lv, W. Yang, W. Huang *et al.*, "Techno-economic of 66 kV AC connection solution for offshore wind power," *Electric Power*, vol. 53, no. 7, pp. 72-79, Jul. 2020.

[21] M. Deriu, M. Migliori, C. Gadaleta *et al.*, "Grid connection of large offshore wind plants: techno-economic evaluation of HVAC solutions," in *Proceedings of 2023 AEIT International Annual Conference*, Rome, Italy, Oct. 2023, pp. 1-6.

[22] F. Fu, H. Li, C. Zhao *et al.*, "Research on adaptive proportional coefficient current limiting control strategy for hybrid MMC," in *Proceedings of 2022 6th International Conference on Green Energy and Applications*, Singapore, Mar. 2022, pp. 154-160.

[23] H. Zhang, W. Xiang, Y. He *et al.*, "Optimal energy utilization of MMC-HVDC system integrating offshore wind farms for onshore weak grid inertia support," *IEEE Transactions on Power Systems*, vol. 39, no. 1, pp. 1304-1318, Jan. 2024.

[24] X. Li, Y. Xu, H. Zhang *et al.*, "Control and protection system design of Zhangbei VSC-HVDC grid," in *Proceedings of 2021 6th Asia Conference on Power and Electrical Engineering*, Chongqing, China, Apr. 2021, pp. 119-123.

Wang Xiang received the B.Eng. and Ph.D. degrees in electrical engineering from Huazhong University of Science and Technology, Wuhan, China, in 2012 and 2017, respectively. He was a visiting Ph.D. student at the University of Aberdeen, Aberdeen, UK and the University of Strathclyde, Glasgow, UK, in 2014 and 2016, respectively. He was with the University of Strathclyde from 2018 to 2021. Currently, he is a Professor at School of Electrical and Electronics Engineering, Huazhong University of Science and Technology. His main research interests include modular multilevel converter based high-voltage direct current (MMC-HVDC), high power DC/DC converter, DC grid, and offshore wind power integration.

Mingrui Yang received the B. E. degree in electrical engineering from South China University of Technology, Guangzhou, China, in 2023. He is currently working toward the M.E. degree in electrical engineering at Huazhong University of Science and Technology, Wuhan, China. His research interests include MMC-HVDC and renewable energy integration.

Jinyu Wen received the B.Eng. and Ph.D. degrees in electrical engineering from Huazhong University of Science and Technology (HUST), Wuhan, China, in 1992 and 1998, respectively. He was a Visiting Student from 1996 to 1997 and Research Fellow from 2002 to 2003 at the University of Liverpool, Liverpool, UK, and a Senior Visiting Researcher at the University of Texas at Arlington, Arlington, USA, in 2010. From 1998 to 2002, he was a Director Engineer in XJ Electric Co., Ltd., Xuchang, China. In 2003, he joined the HUST and now is a Professor at HUST. His current research interests include renewable energy integration, energy storage application, DC grid, and power system operation and control.